

Metformin regulates the LIN28B-mediated JNK/STAT3 signaling pathway through miR-140-3p in subretinal fibrosis

ZHIJUAN HUA^{1,2*}, WENCHANG YANG^{1*}, DONGLI LI¹, YIXIN CUI¹, LU SHEN¹, LINGNA RAO¹, YUXIANG ZHENG¹, QIYING ZHANG¹, WENYI ZENG¹, YI GONG³ and LING YUAN¹

¹Department of Ophthalmology, The First Affiliated Hospital of Kunming Medical University, Kunming, Yunnan 650032; ²Department of Pediatric Ophthalmology, The Affiliated Hospital of Yunnan University, Kunming, Yunnan 650021; ³Department of Physiology, School of Basic Medical Sciences, Kunming Medical University, Kunming, Yunnan 650500, P.R. China

Received January 13, 2023; Accepted August 30, 2023

DOI: 10.3892/etm.2023.12227

Abstract. Subretinal fibrosis (SF) is an important cause of submacular neovascularization that leads to permanent vision loss, but has no effective clinical treatment. The present study examined the influence of metformin on SF, and investigated whether the mechanism involves the microRNA (miR)-140-3p/LIN28B/JNK/STAT3-mediated regulation of oxidative stress, angiogenesis and fibrosis-associated indicators. A mouse model of laser-induced SF was established. In addition, an ARPE-19 fibrotic cell model was established using TGF- β 1. A Cell Counting Kit-8 assay was used to examine cell viability. Flow cytometry was used to measure reactive oxygen species levels, and western blotting was used to detect the levels of proteins associated with epithelial-mesenchymal transition (EMT), signaling and fibrosis. The levels of superoxide dismutase, malondialdehyde, glutathione-peroxidase and catalase were measured using kits. Scratch assays and Transwell assays were used to assess cell migration and invasion, respectively, and reverse transcription-quantitative PCR was used to determine the levels of miR-140-3p and LIN28B. Dual-luciferase assays were used to verify the targeting relationship between miR-140-3p and LIN28B, and coimmunoprecipitation was used to confirm the interaction between LIN28B and JNK. Masson staining and hematoxylin

and eosin staining were used to examine collagenous fibers and the histopathology of eye tissue. In ARPE-19 cells induced by TGF- β 1, metformin promoted miR-140-3p expression and inhibited LIN28B expression and JNK/STAT3 pathway activation, thereby inhibiting oxidative stress, EMT and fibrosis in ARPE-19 cells. The overexpression of LIN28B or treatment with the JNK/STAT3 agonist anisomycin partially reversed the inhibitory effect of metformin on oxidative stress and fibrosis in ARPE-19 cells. The dual-luciferase reporter assay and coimmunoprecipitation assay showed that miR-140-3p targeted the 3' untranslated region of LIN28B mRNA and inhibited LIN28B expression. LIN28B targeted and bound to JNK and regulated the JNK/STAT3 pathway. Therefore, it may be concluded that metformin can promote miR-140-3p expression, inhibit LIN28B and then inhibit the JNK/STAT3 pathway to alleviate SF.

Introduction

Age-related macular degeneration (AMD) is a prime cause of visual impairment and severe vision loss and is one of the top three eye diseases that can result in blindness (1). Subretinal fibrosis (SF) is a pivotal pathologic trait of neovascular AMD (nAMD) (2). The progression of SF can lead to vision loss (3). SF is primarily characterized by an excess of extracellular matrix (ECM) proteins, including collagen and fibronectin (4). SF and ECM components are mainly produced by activated myofibroblasts (5). In retinal diseases, oxidative stress can lead to neurodegeneration and cell loss, which is associated with early disease progression (6). Thus, it is urgently necessary to develop novel therapies for the treatment of SF.

Metformin is a biguanide that has been widely used to treat diabetes since the 1950s (7). In addition to being an antidiabetic drug with low cost and high safety, metformin has also been shown to inhibit the proliferation and migration of human retinal vascular endothelial cells and reduce oxidative stress in cells and various organs (8,9). Furthermore, metformin has been shown to reverse existing pulmonary fibrosis in mice (10) and inhibit the migration and invasion of cancer cells *in vitro* (11). It has also been shown to have a protective effect against several age-associated diseases, and may prevent the

Correspondence to: Ms. Yi Gong, Department of Physiology, School of Basic Medical Sciences, Kunming Medical University, 1168 Chunrong West Road, Kunming, Yunnan 650500, P.R. China
E-mail: 2435136606@qq.com

Dr Ling Yuan, Department of Ophthalmology, The First Affiliated Hospital of Kunming Medical University, 295 Xichang Road, Kunming, Yunnan 650032, P.R. China
E-mail: yuanling@kmmu.edu.cn

*Contributed equally

Key words: metformin, subretinal fibrosis, miR-140-3p, LIN28B, JNK/STAT3

development of AMD (12). Currently, metformin is of interest as a candidate for the treatment of AMD, as it may reduce the progression of AMD via its antioxidant, anti-inflammatory and antifibrotic effects (13). However, the role and mechanism of metformin are intricate, and it is important to determine the mechanism of metformin in the treatment of SF.

MicroRNAs (miRNAs) are small noncoding RNAs that play critical roles in gene regulation and numerous biological processes (14). The development of retinal diseases, including AMD, is associated with the dysregulation of miRNAs and alterations in the mechanisms of miRNA biogenesis (15). Yi *et al* (16) showed that the overexpression of miR-140-3p significantly alleviated inflammation, oxidative stress and apoptosis in oxygen-glucose deprivation and reperfusion models, and exerted a protective effect on cells. In addition, Al-Modawi *et al* (17) showed that miR-140-3p prevented oxidative stress by upregulating the enzyme N(G), N(G)-dimethylarginine dimethylaminohydrolase 1. Furthermore, another study showed that the upregulation of miR-140-3p ameliorated pathological changes and inhibited inflammation, oxidative stress and fibrosis in rats with rheumatoid arthritis (18). These findings indicate that miR-140-3p improves various functions of the body by alleviating oxidative stress and fibrosis. However, the regulatory mechanism of miR-140-3p in SF is unknown.

LIN28 is a reprogramming factor and conserved RNA-binding protein, and the only homolog of LIN28 in humans (19). LIN28B regulates cell migration, invasion, apoptosis and fusion (20). In a study by Liang *et al* (21), LIN28B was shown to induce epithelial-mesenchymal transition (EMT) via the inhibition of let-7d, and the inhibition of LIN28B alleviated TGF- β 1-induced fibrosis. In another study, Zhang and Sui (22) showed that the knockdown of circBPTF mediated the miR-384/LIN28B axis in human umbilical vein endothelial cells, thereby preventing the inflammatory injury and oxidative stress induced by high glucose. Thus, as LIN28B is indicated to regulate fibrosis, the present study investigated the effect of LIN28B on SF.

JNK, which is a Ser/Thr kinase, is a member of the mitogen-activated protein kinase family in mammals. JNK influences multiple cellular processes, including cell proliferation, survival and malignant transformation (23). STAT3 is a cytoplasmic transcription factor that plays a pivotal role in gene expression and is involved in proliferation and survival (24). Yang *et al* (25) showed that JNK enhanced the transcription of TGF- β 1 and connective tissue growth factor and promoted fibrosis in models of acute kidney injury, while the inhibition of JNK activity protected the kidney from the development of fibrosis. Du *et al* (26) demonstrated that the knockdown of atypical protein kinase C- α inhibited the EMT, migration and invasion of colorectal cancer cells by inhibiting the Rac1-JNK pathway. In addition, Zhao *et al* (27) found that STAT3 was intimately associated with the occurrence and development of liver fibrosis induced by multiple factors, and suggested that STAT3 can play an anti-inflammatory or proinflammatory role in the pathogenesis of liver fibrosis. Zhao *et al* (28) also showed that the JNK/STAT3 signaling pathway is involved in the oxidative stress and apoptosis induced by excessive fluoride in female mice, which reduced the development of potential oocytes. These studies offer important information to support exploration of the role of the JNK/STAT3 pathway

in fibrotic diseases and serve as a reference for further study of the mechanism of the JNK/STAT3 pathway in fibrotic diseases.

Therefore, the present study examined the role and effect of metformin in SF, and investigated whether its mechanism involves regulation of the JNK/STAT3 signaling pathway mediated by LIN28B through miR-140-3p. The study may constitute an academic reference for the clinical treatment of SF.

Materials and methods

Establishment and grouping of the animal models. A total of 40 male SPF C57BL/6J mice (18–22 g, 6–8 weeks old) were obtained from the Experimental Animal Center of Yunnan University. The license number for the use of experimental animals was SCXK (Dian) K2021-0002. All procedures were approved by the Experimental Animal Welfare Ethics Committee of the Experimental Animal Center of Yunnan University (Kunming, China; ethics no. YNU20220291). Mice were housed individually using a 12-h light/dark cycle at 22°C with 50% humidity, with food and water available at will, and were domesticated and housed for 1 week prior to the experiment. The mice were randomly divided into 4 groups (n=10/group): Normal control group (mice without laser irradiation), SF group, SF + metformin (SF + Met) group and SF + metformin + miR-140-3p inhibitor group. The mice were anesthetized with pentobarbital sodium (30 mg/kg, intraperitoneal injection), and the laser-induced SF model was examined for 35 days as previously described (29). Briefly, on day 0, the mice were anesthetized with pentobarbital, and 4–6 laser spots (532 nm, 200 mW, 100 msec, 75 μ m; VISULAS® 532s; Zeiss AG) were created in each fundus around the optic disc. Immediately after laser irradiation, a subretinal bubble formed, confirming rupture of the Bruch's membrane. Mice in the two metformin treatment groups were treated with 300 mg/kg/day metformin (Beijing Solarbio Science & Technology Co., Ltd.) by gavage from day 0 to day 35. In addition, the mice in the SF + metformin + miR-140-3p inhibitor group were injected with 5 μ l miR-140-3p inhibitor lentivirus (Hunan Fenghui Biotechnology Co., Ltd., China) through the vitreous cavity on day 0 of laser-induced injury. To administer the intravitreal injection, a 30-gauge needle was first inserted behind the eye margin to make a cavity. The homologous compounds were injected into the incipient well cavities with a 34-gauge Hamilton syringe, and all injections were performed under an operating microscope. Animal health and behavior were monitored every 2 days.

The mice were euthanized on day 35 by decapitation using scissors, and were confirmed dead after decapitation by the loss of heartbeat and breath cessation. Eyeball mouse tissues were collected and fixed in 5% paraformaldehyde for 1 h. The conditions for euthanasia were as follows: i) the end of the animal experiment; ii) the animals were in pain beyond the prespecified mercy end point (such as marked reduction in pre-test body weight, markedly coarse fur, accompanied by unresponsive and behavioral abnormalities, and persistent dyspnea). In addition, meloxicam (1 mg/kg, intragastric administration) was used as an analgesic to minimize the pain and stress of the animals during the experiment.

Cell culture and model construction. The ARPE-19 adult retinal pigment epithelium (RPE) cell line was purchased from Shenzhen Otwo Biotechnology Co., Ltd. and cultured in DMEM/F-12 (MilliporeSigma) containing 10% FBS (MilliporeSigma), 100 U/ml penicillin and 100 µg/ml streptomycin at 37°C with 5% CO₂. The cultured ARPE-19 cells were treated with 10 ng/ml TGF-β1 for 24 and 48 h to establish the fibrotic cell model (TGF-β1 group), and the cells were also cultured with 10 ng/ml TGF-β1 and 2 mM metformin (TGF-β1 + Met group), or 0 ng/ml TGF-β1, 2 mM metformin and 4 µM anisomycin (co-treatment) (TGF-β1 + Met + anisomycin group) for 48 h in subsequent experiments.

Cell transfection. The negative control (NC) mimic, green fluorescent protein miR-140a-3p mimic, miR-140a-3p inhibitor and NC inhibitor were obtained from Sangon Biotech Co., Ltd. ARPE-19 cells were transfected with Lipofectamine™ 2000 (Invitrogen; Thermo Fisher Scientific, Inc.) and the aforementioned nucleic acids (300 ng/µl) for 24 h at 37°C. The transfection efficiency of the miR-140a-3p inhibitor was determined by reverse transcription-quantitative PCR (RT-qPCR) after 36 h. The transfection efficiency of the miR-140a-3p mimic was determined by immunofluorescence using a fluorescence microscope (Leica Microsystems, GmbH) after 36 h.

The lentiviral LIN28B (3rd generation) was obtained from Shanghai GenePharma Co., Ltd. The 293T cell (The Cell Bank of Type Culture Collection of The Chinese Academy of Sciences Cell Bank) used to generate the virions, Packaging plasmids (pMDL, VSVG, REV) were obtained from Shanghai GenePharma Co., Ltd. A mixture comprising 1.5 µg LIN28B plasmid and 1.5 µg packaging plasmid (pMDL:VSVG:REV=5:3:2) was prepared and then added to the culture dish containing 293T cells for 4–6 h (37°C, 5% CO₂). The transfection solution was absorbed and discarded, and fresh culture solution was added for 72 h. Following filtration through a 0.45-µm filter, the virus was collected by ultracentrifugation (4°C, 6,000 × g, 2 h), and the titers were determined by a limited dilution method. One day prior to the experiment, 4 × 10³ ARPE19 cells were inoculated into each well of a 96-well culture plate, and 10 µl 1 × 10⁸ TU/ml virus and 5 µg/ml Polybrene were added to each well (multiplicity of infection, 10) for incubation at 37°C for 24 h. Fluorescence was observed after 72 h of infection. Empty vector was also transfected as the control. The reagents used for lentiviral transfection were provided by Shanghai GenePharma Co., Ltd. The sequences of the NC mimic, miR-140-3p mimic, miR-140-3p inhibitor, NC inhibitor and LIN28B are presented in Table S1.

Cell Counting Kit-8 (CCK-8) analysis of cell proliferation. ARPE-19 cells (5 × 10³ cells/well) were inoculated in a 96-well plate and cultured for 24 h at 37°C in a 5% CO₂ incubator. Following the relevant treatment, 20 µl CCK-8 reagent (Beijing Solarbio Science & Technology Co., Ltd.) was added to the cells in each well. After 2 h of incubation, the absorbance was measured at 450 nm with a microplate reader.

Reactive oxygen species (ROS) detection. ARPE-19 cells were seeded in 6-well plates at 2 × 10⁵ cells/well and incubated with the ROS-specific fluorescent dye dichloro-dihydro-fluorescein

diacetate at 37°C for 0.5 h in the dark. The cells were washed with PBS to remove the unbound dye, digested and then resuspended in 0.5 ml PBS. Finally, ROS levels were determined by FACSCalibur flow cytometry (BD Biosciences) and analyzed with FlowJ software (v10.8.1; BD Biosciences).

The retinal and choroidal tissues of C57BL/6J mice were immediately placed into precooled PBS solution to remove the blood and other pollutants. The tissue was cut into 1-mm³ pieces with ophthalmic scissors and rinsed in precooled PBS to remove the cell fragments. Enzyme digestion solution was added, and digestion was performed in a 37°C constant temperature water bath for 30 min with intermittent oscillation. Digestion was then stopped with precooled PBS, tissue pellets were removed with a 300-mesh nylon mesh filter, and the filtered cells were collected to examine the ROS levels using the aforementioned method.

Western blot analysis. Proteins were isolated from cells or retinchoroidal tissue with RIPA buffer (Beyotime Institute of Biotechnology) containing 1% protease inhibitors. Protein concentrations were determined using a bicinchoninic acid assay (Beijing Solarbio Science & Technology Co., Ltd.) according to the specifications of the kit. A 50-µg quantity of total protein was loaded per lane, and the proteins were separated by SDS-PAGE (5% stacking gel and 10% separating gel), transferred to PVDF membranes (MilliporeSigma) and then blocked with 5% non-fat milk powder for 1.5 h at room temperature. The following diluted primary antibodies were added and incubated overnight at 4°C: E-cadherin (1:1,000; ab231303), vimentin (1:2,000; ab92547), fibronectin (1:3,000; ab2413), N-cadherin (1:5,000; ab76011), JNK (1:1,000; ab76125), phosphorylated (p)-JNK (1:1,000; ab124965), STAT3 (1:1,000; ab68153), p-STAT3 (1:1,000; ab267373), collagen I (1:5,000; ab138492), collagen III (1:1,000; ab184993), LIN28B (1:2,000; ab191881) and β-actin (1:1,000; ab8226) from Abcam and α-smooth muscle actin (SMA; 1:1,000; #192455) Cell Signaling Technology, Inc.). Next, the membranes were incubated with goat anti-rabbit IgG H&L HRP-conjugated secondary antibodies (1:4,000; ab97051; Abcam) for 1 h at room temperature and developed with an ECL kit (Abcam). Finally, the bands were semiquantitatively analyzed using ImageJ 1.52a software (National Institutes of Health).

Superoxide dismutase (SOD), malondialdehyde (MDA), glutathione peroxidase (GSH-PX) and catalase (CAT) assays. An SOD kit (cat. no. BC0170), GSH-PX kit (cat. no. BC1195) and CAT kit (cat. no. BC0200) all from Beijing Solarbio Science & Technology Co., Ltd., and MDA kit (Nanjing Jiancheng Bioengineering Institute), were used to detect the levels of SOD, MDA, GSH-PX and CAT in cells and retinal choroid tissue after processing according to the instructions of the kit manufacturers.

Detection of apoptosis by flow cytometry. Cells in each group were digested with trypsin and rinsed twice with precooled PBS. The apoptosis rate was then determined using an Annexin-V-FITC/PI apoptosis kit (Absin Bioscience, Inc.).

Scratch test. ARPE-19 cells in the logarithmic growth phase were inoculated on 6-well plates after normal digestion and

passage. The cells were scratched with a pipette tip when the cell density reached 90%. The cells were not serum starved, as 1% FBS medium was used to culture with the cells. After 0 and 24 h of culture, cell migration was observed under a light microscope and photographic images were captured.

Transwell assay of cell invasion. Cell invasion experiments were performed using a Transwell chamber (Corning, Inc.). The cell concentration was adjusted to 1×10^5 cells/ml with serum-free DMEM. Then, 200 μ l cell suspension was added to the upper chamber of the Transwell chamber, which was coated with Matrigel (3 h, 37°C) and 600 μ l DMEM containing 10% FBS was added to the lower chamber of the 24-well plate. The cells in the lower chamber were immobilized with 4% paraformaldehyde and stained with crystal violet (Beijing Solarbio Science & Technology Co., Ltd.) after 24 h (37°C) of incubation. The cells were placed under an inverted light microscope, the number of cells at a fixed position in each well were observed, and 5 visual fields were selected for photography and counting.

Coimmunoprecipitation. Cultured cells were homogenized and lysed for 15 min on ice with a mixture of protease inhibitors (Beyotime Institute of Biotechnology) in hypotonic lysis buffer (Beyotime Institute of Biotechnology). The cell lysates were centrifuged at 4,000 \times g for 10 min at 4°C. Following the removal of a small amount of lysate for input western blot analysis, 1 μ g corresponding antibody, anti-Lin28B (1:100; cat. no. ab191881; Abcam) was added to the rest, and the sample was incubated overnight at 4°C with slow shaking. Cell lysates containing 10 μ l protein A agarose beads (Beyotime Institute of Biotechnology) and antibodies were incubated overnight at 4°C. The beads were collected by centrifugation (1,000 \times g, 3 min, 4°C) and washed three times with lysis buffer (Beyotime Institute of Biotechnology). Protein elution was followed by immunoblot analysis.

Dual-luciferase assay. The target binding sites of miR-140-3p and LIN28B were predicted by a bioinformatics database (<http://starbase.sysu.edu.cn/>). Luciferase reporter plasmid (pGL3-Basic/LIN28B WT, pGL3-Basic/LIN28B MUT) was purchased from Shanghai GenePharma Co., Ltd. The LIN28B 3'-untranslated region containing the miR-140-3p binding site was cloned into a pGL3 vector (Promega Corporation) to establish the wild-type LIN28B vector (WT). A site-directed mutagenesis kit was used to generate a mutant LIN28B vector (MUT). WT or MUT was cotransfected with a vector over-expressing miR-140-3p or NC mimic into 293T cells using Lipofectamine™ 3000 (Invitrogen; Thermo Fisher Scientific, Inc.). The luciferase activity was determined using a Promega luciferase reporter system after 48 h, compared with *Renilla* luciferase activity. The Dual-Lumi™ dual luciferase reporter gene detection kit (cat. no. RG088S; Beyotime Institute of Biotechnology) was used, and the experiment was conducted following the manufacturer's instructions.

RT-qPCR. Total RNA was isolated from eye tissues and cells with TRIzol® reagent (cat. no. 15596026; Invitrogen; Thermo Fisher Scientific, Inc.), and cDNA was synthesized by reverse transcription using a First-Strand cDNA synthesis kit

Table I. Primer sequences.

Target	Sequences (5'-3')
miR-140-3p	F: GCGCGTACCACAGGGTAGAA R: AGTGCAGGGTCCGAGGTATT
hsa-LIN28B	F: TAGGAAGTGAAAGAAGACCCAA R: CTGAGGAAACGGTGGTGA
mmu-LIN28B	F: TGTGGACTGTGCGAGAAGAAGA R: CCTGTCTGAGTGCTCTGCCATT
U6	F: GCTTCGGCAGCACATATACTAAAAT R: CGCTTCACGAATTTGCGTGTTCAT
β -actin	F: CACTGTGCCCATCTACGAGG R: TAATGTCACGCACGATTTC

F, forward; R, reverse; miR, microRNA; hsa, *Homo sapiens*; mmu, *Mus musculus*.

(GeneCopoeia, Inc.), with the following temperature protocol: 25°C for 5 min, 42°C for 15 min, 85°C for 5 min and hold at 4°C. RT-qPCR was performed using a SYBR Green real-time fluorescence quantitative PCR kit (Beijing Solarbio Science & Technology Co., Ltd.). The conditions of PCR were as follows: 95°C predenaturation for 30 sec; 40 cycles of 95°C for 15 sec and 60°C for 30 sec; and 72°C extension for 30 sec. The internal reference genes were U6 for miR-140-3p and GAPDH for the other RNAs. Relative expression of miRNA was analyzed by the $2^{-\Delta\Delta C_q}$ method (30). The primer sequences are shown in Table I.

RNA pull-down. Using a Magnetic RNA Protein Pull Down Kit (Thermo Fisher Scientific, Inc.), an RNA pull-down assay was performed in accordance with the manufacturer's instructions. In brief, RNA probes and miR-140-3p were incubated with cell lysate at room temperature. Then magnetic beads were added to form a compound with the probe, which was detected by immunoprecipitation, washing, purification and western blotting.

Hematoxylin and eosin (H&E) staining. After 35 days of treatment, the eyeballs were isolated, enucleated and fixed in FAS eyeball fixative (Wuhan Servicebio Technology Co., Ltd.) for >48 h and then dehydrated and embedded in paraffin. Sections (20- μ m thick) were dewaxed, stained with hematoxylin for 5 min (at room temperature), washed with tap water, stained with eosin for 1 min (at room temperature) and then dehydrated before sealing with neutral gum for observation (light microscopy) and analysis.

Masson staining. Paraffin sections (20- μ m thick) were dewaxed, hydrated with gradient ethanol, stained with hematoxylin for 5 min, and fully washed with water. The sections were then washed with Masson ponceau acid fuchsin solution for 5 min, soaked in 2% glacial acetic acid water, differentiated with 1% phosphomolybdic acid aqueous solution for 3 min without washing and then directly dyed with aniline blue or light green solution for 5 min. After washing with 0.2% glacial acetic acid aqueous solution for 5 sec, 95% alcohol,

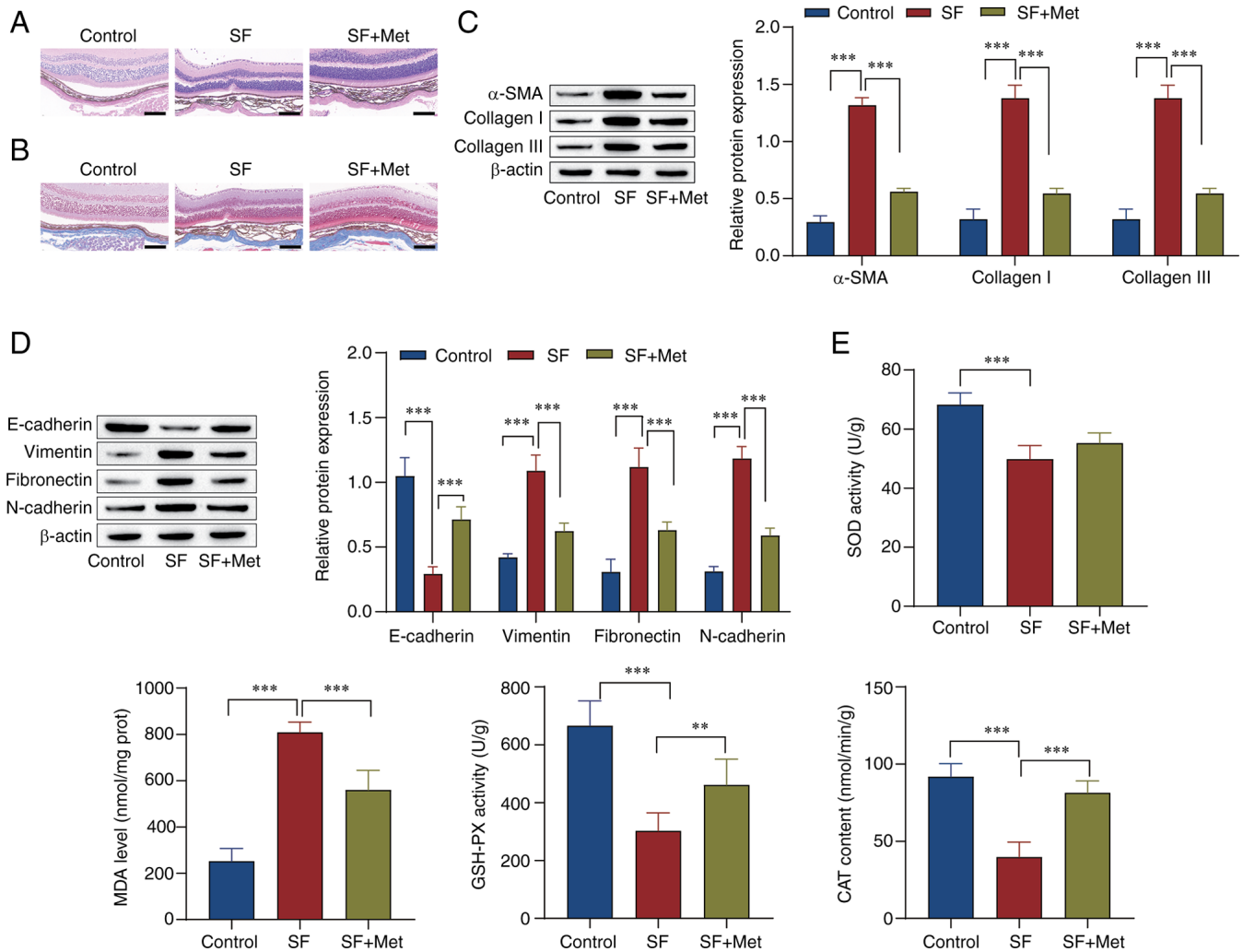


Figure 1. Metformin inhibits the progression of laser-induced subretinal fibrosis in mice. (A) Hematoxylin and eosin staining and (B) Masson staining were used to examine optic cup tissue (scale bar, 100 μ m). Western blotting was performed to examine the levels of (C) fibrosis- and (D) epithelial-mesenchymal transition-associated proteins. (E) Kits were used to examine the levels of SOD, MDA, GSH-PX and CAT. ** $P<0.01$, *** $P<0.001$. Statistical analysis was by one-way ANOVA followed by Tukey's post hoc tests. SOD, superoxide dismutase; MDA, malondialdehyde; GSH-PX, glutathione peroxidase; CAT, catalase; SF, subretinal fibrosis; Met, metformin; SMA, smooth muscle actin; prot, protein.

absolute alcohol, xylene and transparent neutral gum were applied (at room temperature). A light microscope was used to observe and images were captured.

Statistical analysis. GraphPad Prism 8.0 (GraphPad Software; Dotmatics) was used to analyze the experimental data and plot the graphs. The data are from ≥ 3 replicates of all experiments. One-way ANOVA was used for analysis followed by Tukey's post hoc test. $P<0.05$ was considered to indicate a statistically significant result.

Results

Metformin inhibits laser-induced SF and oxidative stress in mice. To examine the effect of metformin on laser-induced SF in mice, the pathology of optic cup tissue was observed using H&E staining. The results showed that compared with the control group, the SF group had more subretinal fibers and fibrocytes and a thickened choroid. However, the subretinal fibers and choroidal thickness were reduced

by metformin (Fig. 1A). Masson staining of the optic cup tissue showed that the amount of collagen fiber synthesis in the SF group was markedly higher than that in the control group, and metformin prominently reduced the synthesis of collagen fibers (Fig. 1B). Western blot analysis showed that the levels of α -SMA, collagen I, collagen III, vimentin, fibronectin and N-cadherin were upregulated in the SF group in comparison with those in the control group, while E-cadherin expression was downregulated. Metformin reversed the effects of SF on these proteins (Fig. 1C and D). Markers of oxidative stress were examined, and the results showed that, in comparison with those in the control group, SOD and GSH-PX activity and CAT content in the SF group were prominently reduced, while the MDA level was increased. The effects in the SF group were reversed by metformin (Fig. 1E). These results indicate that metformin inhibited EMT and fibrosis-associated protein expression, increased the levels of SOD, GSH-PX and CAT, inhibited MDA formation, and alleviated the progression of SF in the mice.

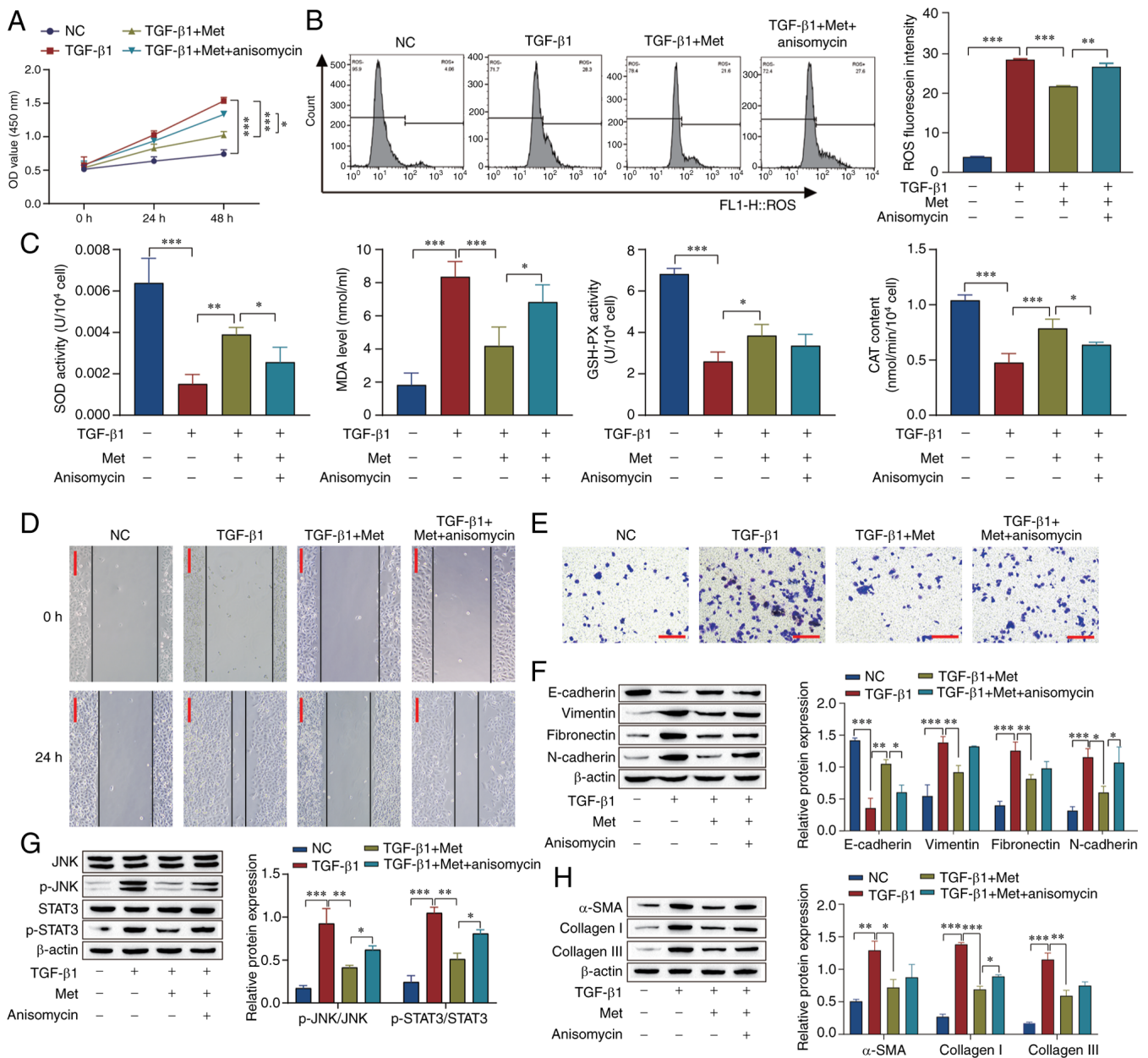


Figure 2. Metformin inhibits fibrosis in retinal pigment epithelial cells through the JNK/STAT3 signaling pathway. (A) A Cell Counting Kit-8 assay was used to examine cell proliferation. (B) ROS levels were detected by flow cytometry. (C) SOD, MDA, GSH-PX and CAT levels in the cells were detected using kits. (D) Scratch tests were used to examine the migration of the cells (scale bar, 100 μ m). (E) Cell invasion was measured using Transwell assays (scale bar, 100 μ m). The expression of (F) epithelial-mesenchymal transition-associated proteins, (G) JNK/STAT3 pathway-associated proteins and (H) fibrosis-related proteins. * P <0.05, ** P <0.01, *** P <0.001. Statistical analysis was by one-way ANOVA followed by Tukey's post hoc tests. ROS, reactive oxygen species; SOD, superoxide dismutase; MDA, malondialdehyde; GSH-PX, glutathione peroxidase; CAT, catalase; NC, negative control; Met, metformin; OD, optical density; p-, phosphorylated; SMA, smooth muscle actin.

Metformin inhibits EMT in RPE cells through the JNK/STAT3 signaling pathway. To examine if the effects of metformin are achieved through the JNK/STAT3 signaling pathway, cell proliferation was examined by CCK-8 assay and ROS levels were measured using flow cytometry. The results showed that cell proliferation and ROS levels were increased in the TGF- β 1 group compared with the NC group. Metformin reversed the effect of TGF- β 1, and anisomycin, an activator of the JNK/STAT3 pathway, attenuated the effect of metformin in both assays (Fig. 2A and B). The oxidative stress level was also examined, and the results showed that in comparison with those in the untreated

control group, the activity of SOD and GSH-PX and the CAT content were reduced, and the levels of MDA were increased in the TGF- β 1 group. The effect of TGF- β 1 was reversed by metformin, while the effect of metformin was attenuated by anisomycin (Fig. 2C). In addition, the results of scratch and Transwell assays showed that the migration and invasion of cells in the TGF- β 1 group were markedly elevated compared with those in the NC group, the effect of TGF- β 1 was reversed by metformin, while the effect of metformin was attenuated by anisomycin (Fig. 2D and E). Furthermore, western blotting showed that TGF- β 1 down-regulated the level of E-cadherin and up-regulated the levels

of vimentin, fibronectin, N-cadherin, p-STAT3/STAT3, p-JNK/JNK, α -SMA, collagen I and collagen III. The effect of TGF- β 1 was reversed by the addition of metformin, and the effect of metformin was attenuated (Fig. 2F-H). These results indicate that the effect of metformin on retinal fibrosis and oxidative stress may involve the JNK/STAT3 pathway.

Metformin inhibits JNK/STAT3 signaling pathway-mediated EMT in RPE cells via miR-140-3p. The levels of miR-140-3p in the RPE cells were measured by RT-qPCR, and the results showed that metformin promoted miR-140-3p expression in the presence of TGF- β 1 (Fig. 3A). Furthermore, the knockdown of miR-140-3p was performed to explore the mechanism of miRNA in the cell model (Fig. 3B). In comparison with that in the TGF- β 1 group, the cell proliferation activity and ROS levels were decreased in the TGF- β 1 + Met group. The effect of TGF- β 1 + Met was attenuated by the miR-140-3p inhibitor (Fig. 3C and D). Compared with those in the TGF- β 1 group, the activity of SOD and GSH-PX and the CAT content were increased, while the MDA levels were decreased in the TGF- β 1 + Met group. The addition of the miR-140-3p inhibitor attenuated the effect of metformin (Fig. 3E). The scratch assay and Transwell results showed that in comparison with those in the NC group, the migration and invasion of cells in the TGF- β 1 group were markedly increased, and the effect of TGF- β 1 was reversed by metformin. The effect observed in the TGF- β 1 + Met group was attenuated by the miR-140-3p inhibitor (Fig. 3F and G). Western blotting showed that in comparison with those in the NC group, the levels of E-cadherin were downregulated and the levels of vimentin, fibronectin, N-cadherin, p-STAT3/STAT3, p-JNK/JNK, α -SMA, collagen I and collagen III were upregulated in the TGF- β 1 group, and the effect of TGF- β 1 was reversed by metformin. Following transfection of the miR-140-3p inhibitor, the effect of metformin in the TGF- β 1 + Met group was reversed (Fig. 3H-J). In summary, these results indicate that metformin inhibits the JNK/STAT3 signaling pathway by promoting miR-140-3p expression, thereby inhibiting RPE cell fibrosis and oxidative stress.

miR-140-3p affects JNK/STAT3 signaling through LIN28B. To further investigate the downstream regulatory mechanism of miR-140-3p, the cells were transfected with miR-140-3p mimic to explore the mechanism of this miRNA in ARPE19 cells. The green fluorescence of the miR-140-3p mimic showed that miR-140-3p was successfully transfected (Fig. 4A). The results of an RNA pull-down assay show that miR-140-3p bonds with LIN28B (Fig. 4B). The binding sites of LIN28B targeted by miR-140-3p were predicted using a bioinformatics website. A dual-luciferase reporter assay confirmed that miR-140-3p downregulated LIN28B (Fig. 4C). To verify whether there was an interactive relationship between LIN28B and JNK, coimmunoprecipitation experiments were performed. The results showed that LIN28B and JNK proteins were precipitated in cells incubated with LIN28B antibody compared with those incubated with IgG antibody (Fig. 4D). RT-qPCR and western blotting results showed transfection with miR-140-3p mimic reduced Lin28B expression (Fig. 4E and F).

miR-140-3p affects TGF- β 1-induced fibrosis in RPE cells through the JNK/STAT3 signaling pathway via LIN28B. ARPE19 cells were transfected with LIN28B overexpression vector, and western blotting results showed that the overexpression of LIN28B was successful (Fig. 5A). In comparison with those in the TGF- β 1 group, the miR-140-3p mimic inhibited cell viability and decreased ROS levels, while LIN28B overexpression attenuated the effect of the mimic in the TGF- β 1 + miR-140-3p mimic group (Fig. 5B and C). In comparison with those in the TGF- β 1 group, the activity of SOD and GSH-PX and the content of CAT were increased, while the levels of MDA were decreased in the cells treated with TGF- β 1 and miR-140-3p mimic. The overexpression of LIN28B reversed the effect of the mimic in the TGF- β 1 + miR-140-3p mimic group (Fig. 5D). As before, the scratch assay and Transwell results showed that cell migration and invasion were increased in the TGF- β 1 group compared with the NC group. Transfection with miR-140-3p mimic reversed the effect of TGF- β 1, while the overexpression of LIN28B attenuated the effect of the mimic in the TGF- β 1 + miR-140-3p mimic group (Fig. 5E and F). Western blotting results indicated that the miR-140-3p mimic inhibited EMT, activation of the JNK/STAT3 pathway and the progression of fibrosis, and the overexpression of LIN28B attenuated these effects (Fig. 5G-I). These results show that overexpression of miR-140-3p inhibited the JNK/STAT3 pathway, thereby inhibiting EMT, the JNK/STAT3 pathway, fibrosis-associated proteins, oxidative stress, cell migration and proliferation, and these effects were inhibited by the overexpression of LIN28B.

Metformin affects SF through miR-140-3p in vivo. Experiments were performed to confirm that the effect of metformin on SF was mediated via miR-140-3p in mice. The RT-qPCR results showed that the miR-140-3p inhibitor was successfully transfected in the mouse eye, and that metformin promoted miR-140-3p expression in SF model mice. In addition, the expression of miR-140-3p was markedly decreased by the miR-140-3p inhibitor (Fig. 6A and B). Western blot analysis showed that the expression levels of α -SMA, collagen I, collagen III, vimentin, fibronectin and N-cadherin were upregulated in the SF group, while E-cadherin expression was downregulated. Metformin reversed the effect of SF on these proteins, while the knockdown of miR-140-3p attenuated the effect of metformin in the SF + Met group (Fig. 6C and D). H&E staining was performed to observe the pathology of the optic cup tissue of the mice. The results showed that compared with the control group, the SF group had greater number of subretinal fibers and fibrocytes, and a thickened choroid. The number of subretinal fibers and choroidal thickness were reduced by metformin. Following the knockdown of miR-140-3p, the formation of subretinal fibers was increased compared with that in the SF + Met group (Fig. 6E). Masson staining of the optic cup tissue showed that the synthesis of collagen fibers in the SF group was markedly higher than that in the control and SF + Met groups, and metformin notably reduced the synthesis of collagen fibers. After miR-140-3p knockdown, collagen fiber synthesis was markedly elevated compared with that in the SF + Met group (Fig. 6F). These results suggest that metformin induced miR-140-3p expression, inhibited EMT -and fibrosis-associated protein expression, thereby alleviating SF in mice.

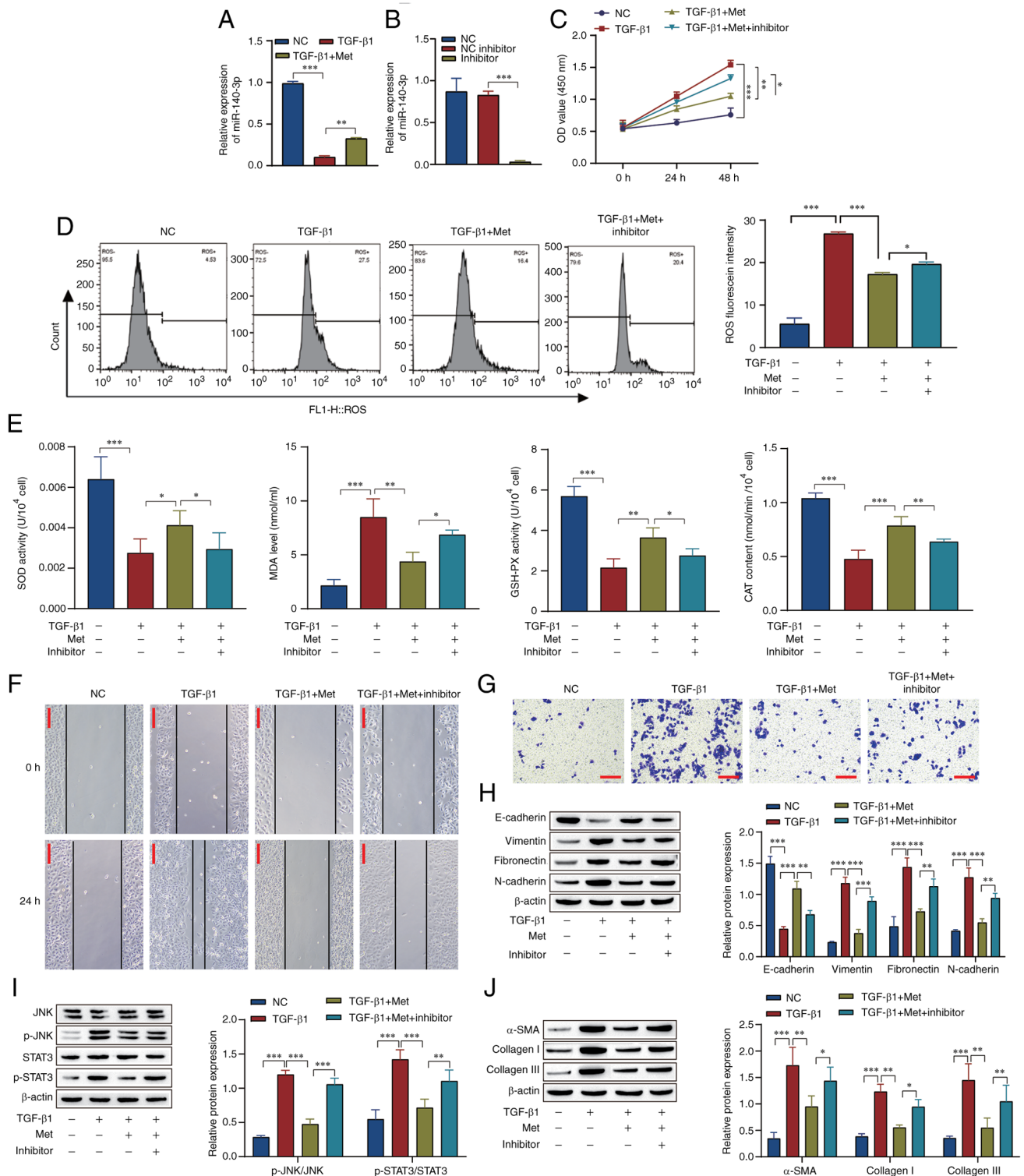


Figure 3. Metformin inhibits JNK/STAT3 signaling pathway-mediated fibrosis in retinal pigment epithelial cells through miR-140-3p. Reverse transcription-quantitative PCR was used to examine miR-140-3p expression in (A) the NC, TGF- β 1 and TGF- β 1 + Met groups and (B) cells transfected with miR-140-3p inhibitor or NC inhibitor. (C) A Cell Counting Kit-8 assay was used to examine cell proliferation. (D) ROS levels were detected by flow cytometry. (E) SOD, MDA, GSH-PX and CAT levels in the cells were detected using kits. (F) Scratch tests were used to examine cell migration (scale bar, 100 μ m). (G) Transwell assays were used to examine cell invasion (scale bar, 100 μ m). Western blot analysis of proteins associated with (H) epithelial-mesenchymal transition, (I) the JNK/STAT3 pathway and (J) fibrosis. * P <0.05, ** P <0.01, *** P <0.001. Statistical analysis was performed by one-way ANOVA followed by Tukey's post hoc tests. NC, negative control; Met, metformin; miR, microRNA; inhibitor, miR-140-3p inhibitor; ROS, reactive oxygen species; SOD, superoxide dismutase; MDA, malondialdehyde; GSH-PX, glutathione peroxidase; CAT, catalase; OD, optical density; p-, phosphorylated; SMA, smooth muscle actin.

Metformin affects the JNK signaling pathway and oxidative stress in SF through miR-140-3p *in vivo*. Whether the effect of metformin on the JNK signaling pathway and oxidative stress

in SF is mediated via miR-140-3p was examined *in vivo*. The RT-qPCR results showed that metformin inhibited LIN28B expression, and the expression level of LIN28B was increased

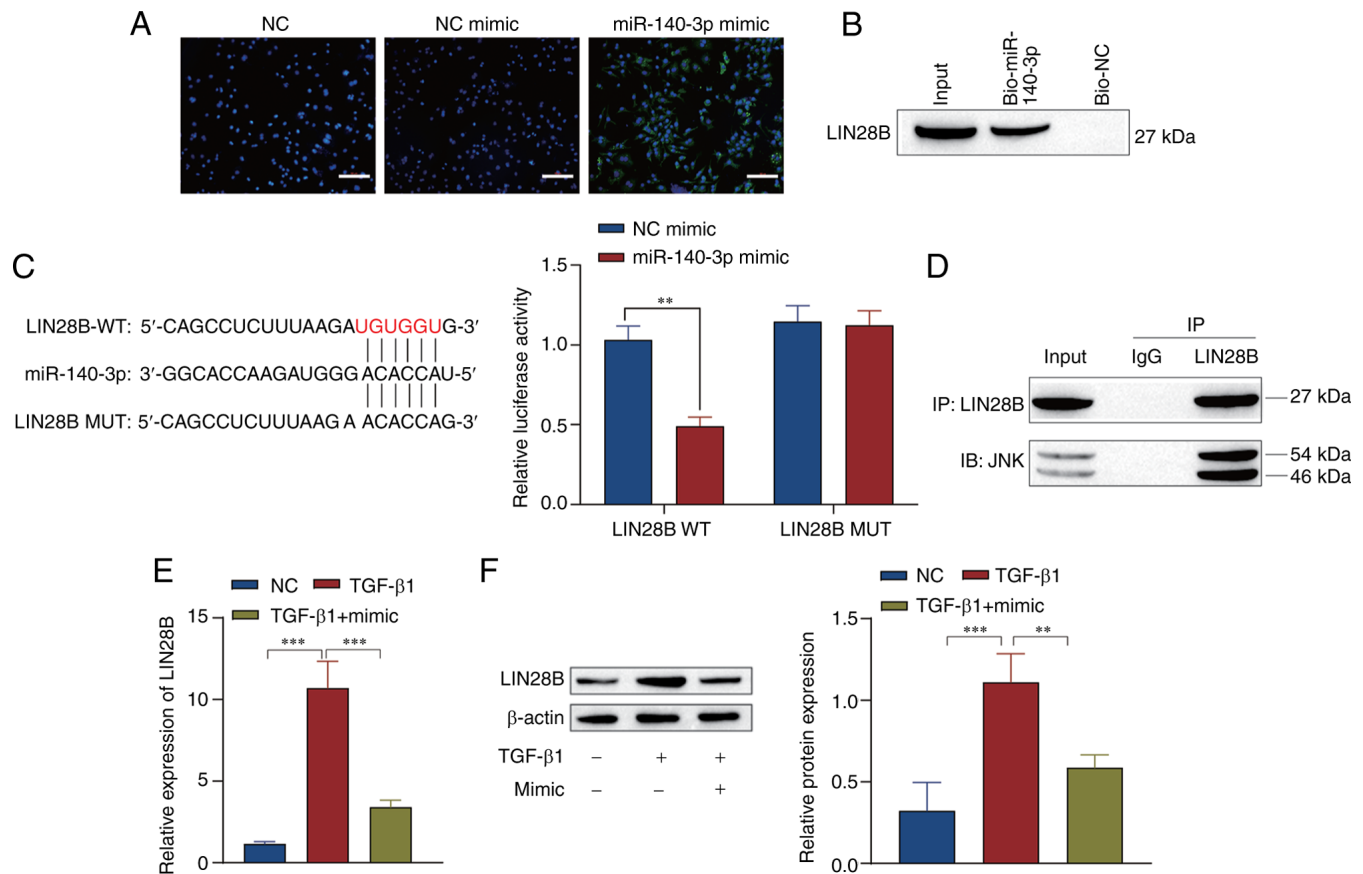


Figure 4. miR-140-3p affects the JNK/STAT3 signaling pathway through LIN28B. (A) Immunofluorescence was used to confirm transfection with miR-140-3p mimic (scale bar, 100 μ m). (B) RNA pull-down assay confirmed the targeting relationship between miR-140-3p and LIN28B. (C) StarBase was used to predict the sequences of the binding sites of miR-140-3p and LIN28B, and a dual-luciferase assay was performed to confirm the targeting relationship between miR-140-3p and LIN28B. (D) The interaction between LIN28B and JNK was verified by coimmunoprecipitation assay. (E) Reverse transcription-quantitative PCR and (F) western blot analysis of the expression of LIN28B. ** $P < 0.01$, *** $P < 0.001$. Statistical analysis was performed by (C) two-way ANOVA and (E and F) one-way ANOVA followed by Tukey's post hoc tests. miR, microRNA; NC, negative control; WT, wild type; MUT, mutant; IP, immunoprecipitation; IB, immunoblotting; mimic, miR-140-3p mimic.

by miR-140-3p inhibitor treatment (Fig. 7A). Western blot analysis showed that p-STAT3 and p-JNK were upregulated in the SF group compared with the control group, and metformin attenuated STAT3 and JNK phosphorylation levels compared with those in the SF group. In addition, the knockdown of miR-140-3p reversed the effect of metformin in the SF + Met group (Fig. 7B). Flow cytometry results showed that metformin reversed the effect of SF modeling on ROS levels, while the knockdown of miR-140-3p reversed the effect of metformin in the SF + Met group (Fig. 7C). In addition, the activity of SOD and GSH-PX and the content of CAT were reduced while the levels of MDA were increased in the SF group compared with the control group. The effects observed in the SF group were reversed by metformin, and those observed the SF + Met group were attenuated by the knockdown of miR-140-3p (Fig. 7D). These results indicate that metformin inhibited the JNK signaling pathway and oxidative stress via the inhibition of LIN28B expression, and the changes induced by metformin were reversed by knocking down miR-140-3p.

Discussion

Fibrosis is a pathologic trait of most chronic inflammatory diseases, which affects almost all tissues and can eventually

lead to organ dysfunction and death (31). SF is a vascularized lesion with abundant immune cells, myofibroblasts, ECM protein sedimentation and EMT (6,32,33). SF damages photoreceptors, the RPE and choroidal capillaries, leading to irreversible loss of central vision (5). To date, no effective antifibrotic therapy to reduce SF formation in patients with nAMD has been discovered (5). Therefore, it is imperative to further study the pathogenesis of SF and identify novel and more effective treatments for SF.

Metformin, which is a potent AMP-activated protein kinase (AMPK) activator, has emerged as a promising agent for the reduction or reversal of fibrosis (34). This agent also has antioxidant and anti-inflammatory effects (35). Kheirollahi *et al* (36) showed that metformin accelerated the regression of fibrosis in the lung by inducing the transdifferentiation of myofibroblasts into adipofibroblasts. Metformin has also been shown to attenuate renal fibrosis induced by unilateral ureteral obstruction in AMPK α 2-deficient mice (37). In the present study, a laser-induced SF model was established in mice and the optic cup tissue of the mice was examined by H&E and Masson staining. The results indicated that metformin effectively alleviated SF in mice.

JNK and STAT3 mediate cell transformation, proliferation, survival and migration (23,38). The JNK/STAT3 pathway has

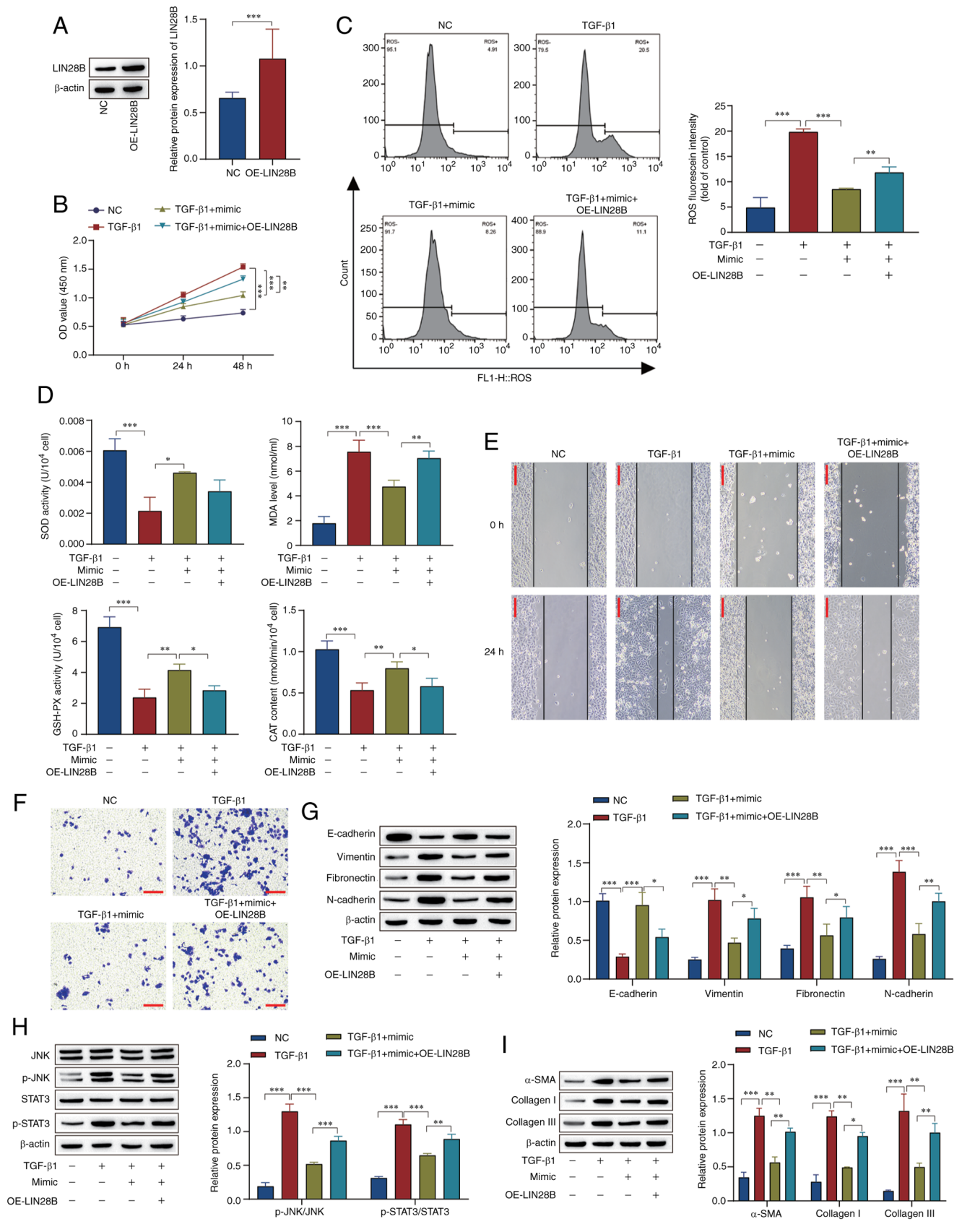


Figure 5. miR-140-3p affects TGF- β 1-induced retinal pigment epithelial cell fibrosis through the JNK/STAT3 signaling pathway via LIN28B. (A) Expression of LIN28B in transfected cells was measured by western blotting. (B) Cell Counting Kit-8 analysis of cell proliferation. (C) Flow cytometric analysis of ROS levels. (D) SOD, MDA, GSH-PX and CAT levels were detected using kits. (E) Scratch tests were used to examine cell migration (scale bar, 100 μ m). (F) Transwell assays were used to examine cell invasion (scale bar, 100 μ m). Western blot analysis of proteins associated with (G) epithelial-mesenchymal transition, (H) the JNK/STAT3 signaling pathway and (I) fibrosis. * $P < 0.05$, ** $P < 0.01$, *** $P < 0.001$. Statistical analysis was performed by one-way ANOVA followed by Tukey's post hoc tests. miR, microRNA; ROS, reactive oxygen species; SOD, superoxide dismutase; MDA, malondialdehyde; GSH-PX, glutathione peroxidase; CAT, catalase; NC, negative control; OE, overexpression; mimic, miR-140-3p mimic; OD, optical density; p-, phosphorylated; SMA, smooth muscle actin.

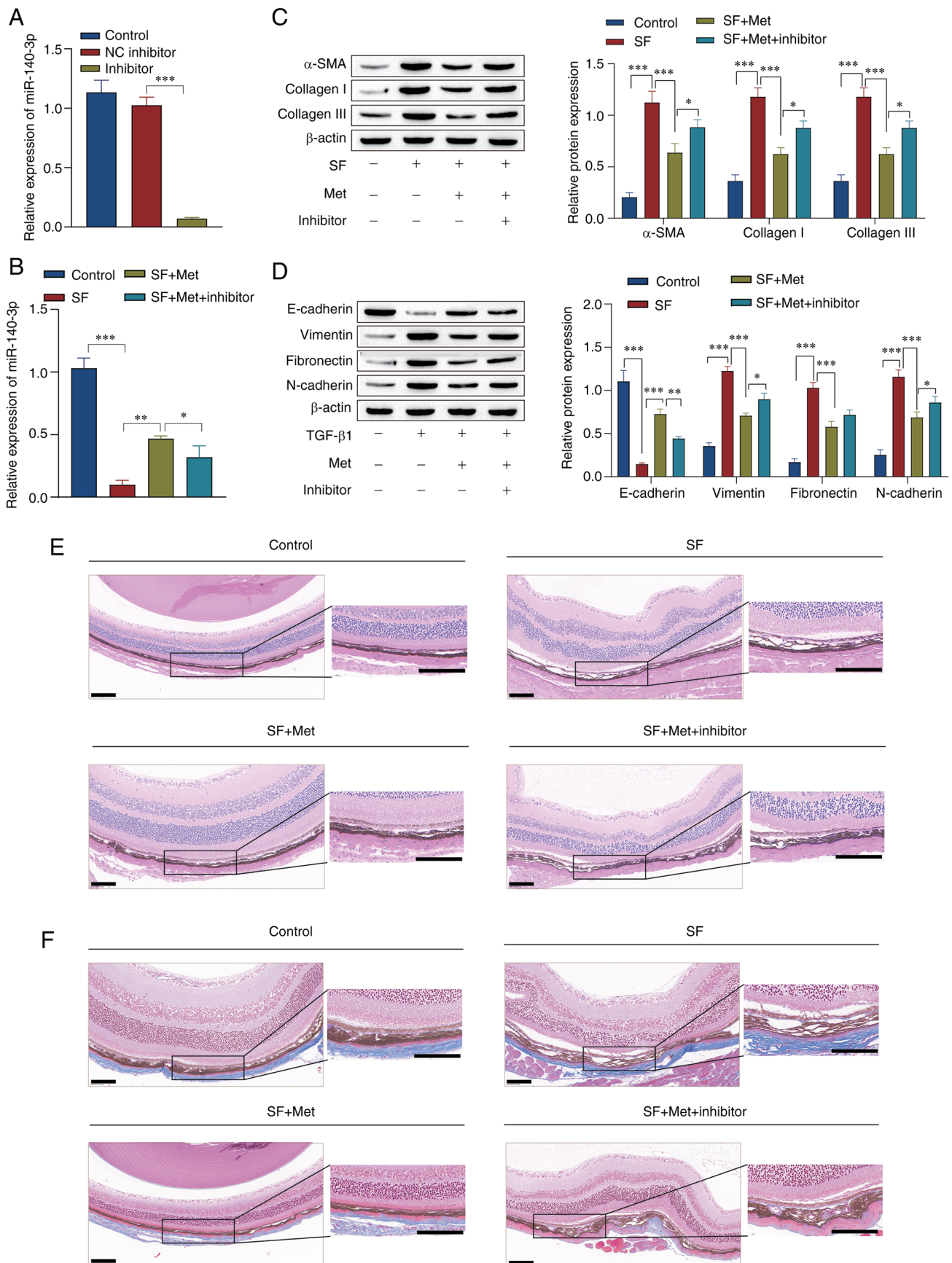


Figure 6. Experiments using mice verified that metformin affects subretinal fibrosis through miR-140-3p. Reverse transcription-quantitative PCR was used to measure the level of miR-140-3p to (A) confirm transfection with miR-140-3p inhibitor and (B) compare its expression in different groups. Western blot analysis of the expression levels of proteins associated with (C) fibrosis and (D) epithelial-mesenchymal transition. (E) Hematoxylin and eosin staining was used to observe pathological changes in optic cup tissue (scale bar, 100 μ m). (F) Masson staining of optic cup tissue (scale bar, 100 μ m). * P <0.05, ** P <0.01, *** P <0.001. Statistical analysis was performed by one-way ANOVA followed by Tukey's post hoc tests. miR, microRNA; NC, negative control; inhibitor, miR-140-3p inhibitor; SF, subretinal fibrosis; Met, metformin; SMA, smooth muscle actin.

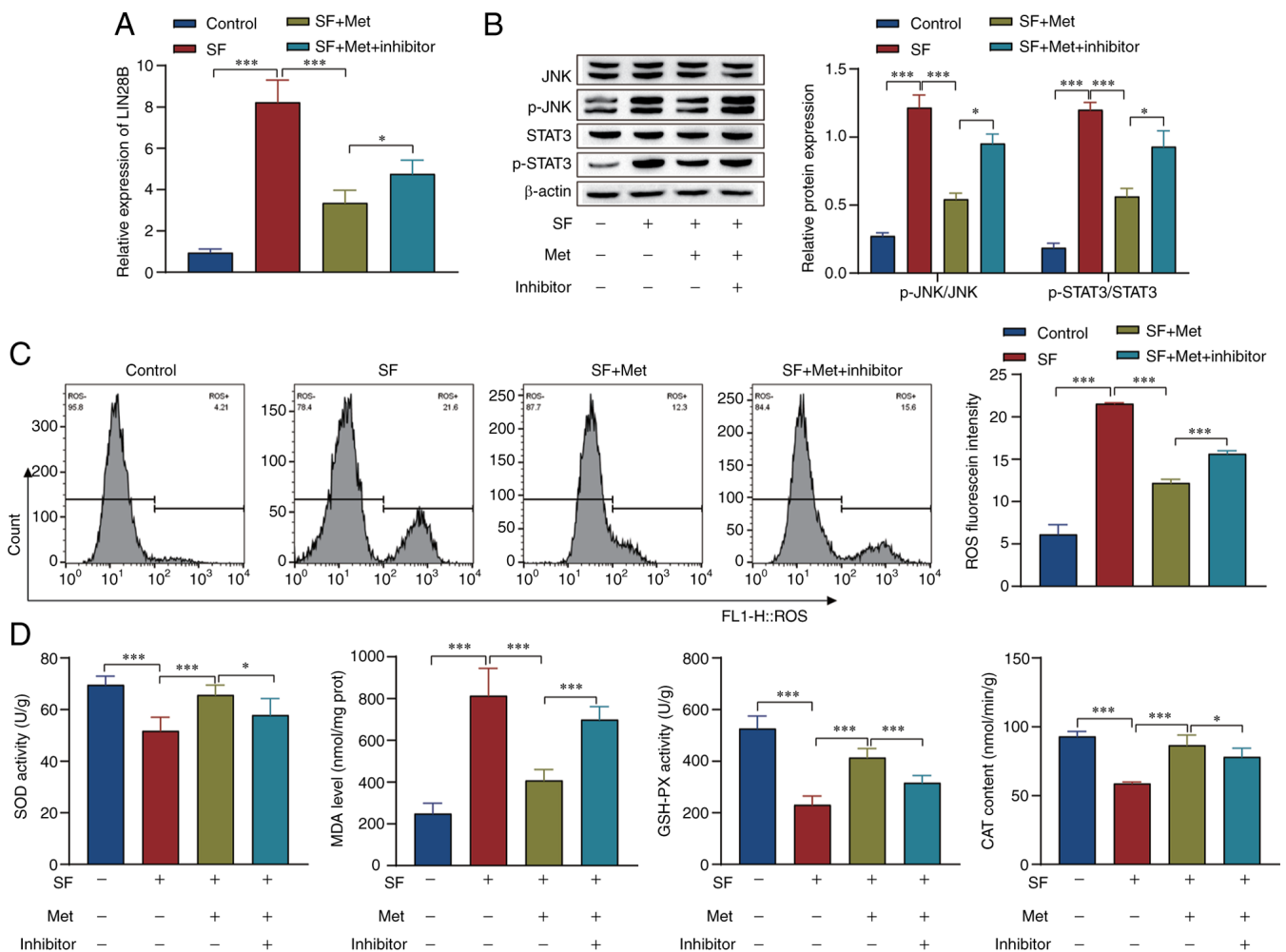


Figure 7. Experiments using mice verified that metformin affects the JNK signaling pathway and oxidative stress levels in subretinal fibrosis through miR-140-3p. (A) Reverse transcription-quantitative PCR was used to examine the level of LIN28B in the different treatment groups. (B) Western blot analysis of the levels of JNK/STAT3 pathway-associated proteins. (C) Levels of ROS were detected by flow cytometry. (D) Kits were used to examine the levels of SOD, MDA, GSH-PX and CAT. * $P < 0.05$, *** $P < 0.001$. Statistical analysis was performed by one-way ANOVA followed by Tukey's post hoc tests. Inhibitor, miR-140-3p inhibitor; miR, microRNA; OD, superoxide dismutase; MDA, malondialdehyde; GSH-PX, glutathione peroxidase; CAT, catalase; SF, subretinal fibrosis; Met, metformin; p-, phosphorylated; ROS, reactive oxygen species; prot, protein.

been reported to contribute to numerous diseases; for example, Wang *et al* (39) showed that the JNK/STAT3 pathway is involved in the formation of ECM in scar tissue after tendon injury. In addition, Yan *et al* (40) and Zhao *et al* (28) showed that the JNK/STAT3 pathway plays a role in the regulation of oxidative stress and apoptosis. Furthermore, Dong *et al* (41) showed that metformin significantly attenuated the fibrotic activity of hepatic stellate cells induced by injury in hepatocellular carcinoma cells by targeting JNK *in vivo*. In the present study, the results showed that JNK/STAT3 pathway proteins were highly activated in SF mouse and cell models, suggesting that the JNK/STAT3 pathway may be involved in the occurrence and development of SF. Further experiments indicated that metformin inhibited EMT and fibrosis-associated protein expression, cell migration, invasion and proliferation, and reduced ROS and MDA levels by inhibiting the JNK/STAT3 signaling pathway. The levels of SOD, GSH-PX and CAT were also increased, which may be associated with the inhibition of fibrosis in RPE cells.

miRNAs have been shown to regulate organ fibrosis by modulating the activity of relevant signaling pathways (42).

For example, it has been shown that miR-144-3p and miR-328 are involved in the regulation of cardiac fibrosis, and miR-34a and miR-17-5p contribute to the development of liver fibrosis under different conditions (42). Wu *et al* (18) indicated that miR-140-3p is a mediator of hepatic stellate cell proliferation, and its knockdown inhibited the TGF- β 1-induced proliferation and fibrosis of HSC-T6 cells. In addition, Zhang *et al* (43) showed that the overexpression of miR-140-3p inhibited EMT, invasion and metastasis in hepatocellular carcinoma. In the present study, it was found that miR-140-3p was expressed at low levels in SF mouse and cell models, and the expression level of miR-140-3p was markedly elevated after metformin treatment. The upregulation of miR-140-3p expression by metformin was associated with inhibition of JNK/STAT3 pathway activation and EMT- and fibrosis-associated protein expression, increases in the levels of SOD, GSH-PX and CAT, and inhibition of MDA production and SF in cells and animals.

LIN28 is a highly conserved RNA-binding protein that has two homologs: LIN28A and LIN28B. Lin28B deficiency has been shown to increase let-7a/let-7b expression and decrease hepatic stellate cell activation and liver fibrosis

in mice with alcoholic liver injury (44). In addition, a study by Lu *et al* (45) showed that the overexpression of LIN28B activated the STAT3 signaling pathway in lung cancer, thus promoting EMT and accelerating migration and invasion. In the present study, the relationship between LIN28B and the JNK/STAT3 pathway was examined. The results demonstrated an interaction between LIN28B and JNK. Overexpression of LIN28B was also shown to upregulate the phosphorylation of JNK/STAT3 pathway-related proteins and induce activation of the JNK/STAT3 pathway. Moreover, the results of the double luciferase experiment indicated that miR-140-3p targets LIN28B.

In summary, the present study indicated that metformin inhibits SF by facilitating miR-140-3p expression and inhibiting LIN28B and the JNK/STAT3 pathway at the cellular and organismal levels. The study may be considered as a novel academic reference for those interested the treatment of SF. However, the mechanism was only examined in cell and mouse experiments, and it remains to be further studied whether there are any adverse reactions or side effects of this treatment in clinical use.

Acknowledgements

Not applicable.

Funding

The study was supported by The Applied Basic Research Foundation of the Department of Science, Technology of Yunnan Province, Yunnan, China (grant no. 202201AY070001-036), the National Natural Science Foundation Project (grant no. 82260207) and Scientific Research Fund of Education Department of Yunnan Province (grant no. 2023J0036).

Availability of data and materials

The datasets used and/or analyzed during the current study are available from the corresponding author on reasonable request.

Authors' contributions

ZH, WY, YG and DL were responsible for conceptualization of the study. ZH, WY and YC were responsible for methodology. ZH and WY performed validations. ZH, WY, LS and LR carried out the formal analysis. ZH, WY, YG and LY performed investigations, wrote the original draft of the manuscript, reviewed and edited the manuscript and supervised the study. LY provided resources and acquired funding. YZ, QZ and WZ were responsible for visualization and data analysis. ZH and LY confirm the authenticity of all the raw data. All authors read and approved the final version of the manuscript.

Ethics approval and consent to participate

All animal experimental protocols were approved by the Laboratory Animal Welfare Ethics Committee of Yunnan University (approval no. YNU20220291), and the animal procedures are reported according to ARRIVE guidelines 2.0.

Patient consent for publication

Not applicable.

Competing interests

The authors declare that they have no competing interests.

References

1. Mitchell P, Liew G, Gopinath B and Wong TY: Age-related macular degeneration. *Lancet* 392: 1147-1159, 2018.
2. Ma X, Takahashi Y, Wu W, Chen J, Dehdarani M, Liang W, Shin YH, Benyajati S and Ma JX: Soluble very low-density lipoprotein receptor (sVLDLR) inhibits fibrosis in neovascular age-related macular degeneration. *FASEB J* 35: e22058, 2021.
3. Zhou L, Shi DP, Chu WJ, Yang LL and Xu HF: LRG1 promotes epithelial-mesenchymal transition of retinal pigment epithelium cells by activating NOX4. *Int J Ophthalmol* 14: 349-355, 2021.
4. Zhang C, Qin S, Xie H, Qiu Q, Wang H, Zhang J, Luo D and Zhang J: RO4929097, a selective γ -secretase inhibitor, inhibits subretinal fibrosis via suppressing notch and ERK1/2 signaling in laser-induced mouse model. *Invest Ophthalmol Vis Sci* 63: 14, 2022.
5. Tenbrock L, Wolf J, Boneva S, Schlecht A, Agostini H, Wieghofer P, Schlunck G and Lange C: Subretinal fibrosis in neovascular age-related macular degeneration: Current concepts, therapeutic avenues, and future perspectives. *Cell Tissue Res* 387: 361-375, 2022.
6. Mueller-Buehl AM, Doepper H, Grauthoff S, Kiebler T, Peters L, Hurst J, Kuehn S, Bartz-Schmidt KU, Dick HB, Joachim SC and Schnichels S: Oxidative stress-induced retinal damage is prevented by mild hypothermia in an ex vivo model of cultivated porcine retinas. *Clin Exp Ophthalmol* 48: 666-681, 2020.
7. Flory J and Lipska K: Metformin in 2019. *JAMA* 321: 1926-1927, 2019.
8. Han J, Li Y, Liu X, Zhou T, Sun H, Edwards P, Gao H, Yu FS and Qiao X: Metformin suppresses retinal angiogenesis and inflammation in vitro and in vivo. *PLoS One* 13: e0193031, 2018.
9. Wang G, Chen S, Shao Z, Li Y, Wang W, Mao L, Li J and Mei X: Metformin alleviates hydrogen peroxide-induced inflammation and oxidative stress via inhibiting P2X7R signaling in spinal cord tissue cells neurons. *Can J Physiol Pharmacol* 99: 768-774, 2021.
10. Rangarajan S, Bone NB, Zmijewska AA, Jiang S, Park DW, Bernard K, *et al*. Metformin reverses established lung fibrosis in a bleomycin model. *Nature Medicine* 24: 1121-7, 2018.
11. Lv Z and Guo Y: Metformin and its benefits for various diseases. *Front Endocrinol (Lausanne)* 11: 191, 2020.
12. Blitzer AL, Ham SA, Colby KA and Skondra D: Association of metformin use with age-related macular degeneration: A case-control study. *JAMA Ophthalmol* 139: 302-309, 2021.
13. Romdhoniyah DF, Harding SP, Cheyne CP and Beare NAV: Metformin, a potential role in age-related macular degeneration: A systematic review and meta-analysis. *Ophthalmol Ther* 10: 245-260, 2021.
14. Zhang L, Chen T, Yin Y, Zhang CY and Zhang YL: Dietary microRNA-A novel functional component of food. *Adv Nutr* 10: 711-721, 2019.
15. Askou AL, Alsing S, Holmgaard A, Bek T and Corydon TJ: Dissecting microRNA dysregulation in age-related macular degeneration: New targets for eye gene therapy. *Acta Ophthalmol* 96: 9-23, 2018.
16. Yi M, Li Y, Wang D, Zhang Q, Yang L and Yang C: KCNQT1 exacerbates ischemia-reperfusion injury through targeted inhibition of miR-140-3P. *Inflammation* 43: 1832-1845, 2020.
17. Al-Modawi RN, Brinchmann JE and Karlsen TA: Multi-pathway protective effects of MicroRNAs on human chondrocytes in an in vitro model of osteoarthritis. *Mol Ther Nucleic Acids* 17: 776-790, 2019.
18. Wu SM, Li TH, Yun H, Ai HW and Zhang KH: miR-140-3p knockdown suppresses cell proliferation and fibrogenesis in hepatic stellate cells via PTEN-mediated AKT/mTOR signaling. *Yonsei Med J* 60: 561-569, 2019.

19. Zhou J, Ng SB and Chng WJ: LIN28/LIN28B: An emerging oncogenic driver in cancer stem cells. *Int J Biochem Cell Biol* 45: 973-978, 2013.
20. Huang Q, Niu Y, Song L, Huang J, Wang C and Ma T: Does LIN28B gene dysregulation make women more likely to abort? *Reprod Fertil* 2: 211-220, 2021.
21. Liang H, Liu S, Chen Y, Bai X, Liu L, Dong Y, Hu M, Su X, Chen Y, Huangfu L, *et al*: miR-26a suppresses EMT by disrupting the Lin28B/let-7d axis: Potential cross-talks among miRNAs in IPF. *J Mol Med (Berl)* 94: 655-665, 2016.
22. Zhang W and Sui Y: CircBPTF knockdown ameliorates high glucose-induced inflammatory injuries and oxidative stress by targeting the miR-384/LIN28B axis in human umbilical vein endothelial cells. *Mol Cell Biochem* 471: 101-111, 2020.
23. Miyazaki T, Bub JD and Iwamoto Y: c-Jun NH(2)-terminal kinase mediates leptin-stimulated androgen-independent prostate cancer cell proliferation via signal transducer and activator of transcription 3 and Akt. *Biochim Biophys Acta* 1782: 593-604, 2008.
24. Guo ZL, Li JZ, Ma YY, Qian D, Zhong JY, Jin MM, Huang P, Che LY, Pan B, Wang Y, *et al*: Shikonin sensitizes A549 cells to TRAIL-induced apoptosis through the JNK, STAT3 and AKT pathways. *BMC Cell Biol* 19: 29, 2018.
25. Yang L, Besschetnova TY, Brooks CR, Shah JV and Bonventre JV: Epithelial cell cycle arrest in G2/M mediates kidney fibrosis after injury. *Nat Med* 16: 535-543, 1p, 143, 2010.
26. Du GS, Qiu Y, Wang WS, Peng K, Zhang ZC, Li XS, Xiao WD and Yang H: Knockdown on aPKC- ι inhibits epithelial-mesenchymal transition, migration and invasion of colorectal cancer cells through Rac1-JNK pathway. *Exp Mol Pathol* 107: 57-67, 2019.
27. Zhao J, Qi YF and Yu YR: STAT3: A key regulator in liver fibrosis. *Ann Hepatol* 21: 100224, 2021.
28. Zhao WP, Wang HW, Liu J, Tan PP, Lin L and Zhou BH: JNK/STAT signalling pathway is involved in fluoride-induced follicular developmental dysplasia in female mice. *Chemosphere* 209: 88-95, 2018.
29. Ishikawa K, Kannan R and Hinton DR: Molecular mechanisms of subretinal fibrosis in age-related macular degeneration. *Exp Eye Res* 142: 19-25, 2016.
30. Livak KJ and Schmittgen TD: Analysis of relative gene expression data using real-time quantitative PCR and the 2(-Delta Delta C(T)) method. *Methods* 25: 402-408, 2001.
31. Wynn TA and Ramalingam TR: Mechanisms of fibrosis: Therapeutic translation for fibrotic disease. *Nat Med* 18: 1028-1040, 2012.
32. Yi C, Liu J, Deng W, Luo C, Qi J, Chen M and Xu H: Macrophage elastase (MMP12) critically contributes to the development of subretinal fibrosis. *J Neuroinflammation* 19: 78, 2022.
33. Li D, Zhang J, Liu Z, Gong Y and Zheng Z: Human umbilical cord mesenchymal stem cell-derived exosomal miR-27b attenuates subretinal fibrosis via suppressing epithelial-mesenchymal transition by targeting HOXC6. *Stem Cell Res Ther* 12: 24, 2021.
34. Wu M, Xu H, Liu J, Tan X, Wan S, Guo M, Long Y and Xu Y: Metformin and fibrosis: A review of existing evidence and mechanisms. *J Diabetes Res* 2021: 6673525, 2021.
35. Khateeb J, Fuchs E and Khamaisi M: Diabetes and lung disease: A neglected relationship. *Rev Diabet Stud* 15: 1-15, 2019.
36. Kheirollahi V, Wasnick RM, Biasin V, Vazquez-Armendariz AI, Chu X, Moiseenko A, Weiss A, Wilhelm J, Zhang JS, Kwapiszewska G, *et al*: Metformin induces lipogenic differentiation in myofibroblasts to reverse lung fibrosis. *Nat Commun* 10: 2987, 2019.
37. Feng Y, Wang S, Zhang Y and Xiao H: Metformin attenuates renal fibrosis in both AMPK α 2-dependent and independent manners. *Clin Exp Pharmacol Physiol* 44: 648-655, 2017.
38. Haura EB, Turkson J and Jove R: Mechanisms of disease: Insights into the emerging role of signal transducers and activators of transcription in cancer. *Nat Clin Pract Oncol* 2: 315-324, 2005.
39. Wang Y, He G, Tang H, Shi Y, Kang X, Lyu J, Zhu M, Zhou M, Yang M, Mu M, *et al*: Aspirin inhibits inflammation and scar formation in the injury tendon healing through regulating JNK/STAT-3 signalling pathway. *Cell Prolif* 52: e12650, 2019.
40. Yan QL, Wang XY, Bai M, Zhang X, Song SJ and Yao GD: Sesquiterpene lactones from *Elephantopus scaber* exhibit cytotoxic effects on glioma cells by targeting GSTP1. *Bioorg Chem* 129: 106183, 2022.
41. Dong G, Ma M, Lin X, Liu H, Gao D, Cui J, Ren Z and Chen R: Treatment-damaged hepatocellular carcinoma promotes activities of hepatic stellate cells and fibrosis through GDF15. *Exp Cell Res* 370: 468-477, 2018.
42. Ghafouri-Fard S, Abak A, Talebi SF, Shoorei H, Branicki W, Taheri M and Akbari Dilmaghani N: Role of miRNA and lncRNAs in organ fibrosis and aging. *Biomed Pharmacother* 143: 112132, 2021.
43. Zhang QY, Men CJ and Ding XW: Upregulation of microRNA-140-3p inhibits epithelial-mesenchymal transition, invasion, and metastasis of hepatocellular carcinoma through inactivation of the MAPK signaling pathway by targeting GRN. *J Cell Biochem* 120: 14885-14898, 2019.
44. McDaniel K, Huang L, Sato K, Wu N, Annable T, Zhou T, Ramos-Lorenzo S, Wan Y, Huang Q, Francis H, *et al*: The let-7/Lin28 axis regulates activation of hepatic stellate cells in alcoholic liver injury. *J Biol Chem* 292: 11336-11347, 2017.
45. Lu YY, Lin Y, Ding DX, Su S, Chi QQ, Zhang YC, Sun J, Zhang X, Zhu HM, Huang QS, *et al*: MiR-26a functions as a tumor suppressor in ambient particulate matter-bound metal-triggered lung cancer cell metastasis by targeting LIN28B-IL6-STAT3 axis. *Arch Toxicol* 92: 1023-1035, 2018.



Copyright © 2023 Hua *et al*. This work is licensed under a Creative Commons Attribution-NonCommercial-NoDerivatives 4.0 International (CC BY-NC-ND 4.0) License.